Nanoscale

PAPER

View Article Online
View Journal

Cite this: DOI: 10.1039/d3nr02760k

Disclosing gate-opening/closing events inside a flexible metal–organic framework loaded with CO_2 by reactive and essential dynamics†

Susanna Monti, *[a] Cheherazade Trouki [b,c] and Giovanni Barcaro[b]

Received 10th June 2023,
Accepted 14th August 2023

DOI: 10.1039/d3nr02760k

rsc.li/nanoscale

We have combined reactive molecular dynamics simulations with principal component analysis to provide a clearer view of the interactions and motion of the CO_2 molecules inside a metal–organic framework and the movements of the MOF components that regulate storage, adsorption, and diffusion of the guest species. The tens-of-nanometer size of the simulated model, the capability of the reactive force field tuned to reproduce the inorganic–organic material confidently, and the unconventional use of essential dynamics have effectively disclosed the gate-opening/closing phenomenon, possible coordinations of CO_2 at the metal centers, all the diffusion steps inside the MOF channels, the primary motions of the linkers, and the effects of their concerted rearrangements on local CO_2 relocations.

1 Introduction

As versatile porous materials containing metal and organic components, metal–organic frameworks (MOF) are increasingly used for gas entrapment, separation, and conversion.[1–4] Even though they are solids with ordered inorganic binding units (IBU), these are connected by relatively flexible ligands. The degree of flexibility of a MOF and its dynamics depend on the linkers' choice. Self-interactions and the interactions of the linkers with the guest molecules control the MOF function; thus, appropriate functionalizations or structural modifications could be introduced to regulate these properties for optimal performance.[5,6] Indeed, tuned librations/rotations of the organic portions and even specific reactivity could affect the trapping/storing times and conversion of the guests, especially in the case of CO_2. In ref. 7 and references therein, for example, the authors discussed the importance of the selectivity of MOFs relative to the physisorption/chemisorption of CO_2. They explained that the first process, as a weak connection (vdW type) to the MOF surface, reversible and exothermic, maintains the molecule's structure and plays a role in the MOF separation ability. In this case, the MOF pores size should be evaluated and compared with the kinetic size of CO_2 to demonstrate the MOF selectivity for this molecule. Thus, it is crucial to identify the MOF pores and tunnels and describe the dynamics of their size (morphological changes). The chemisorption process, implying the formation of a chemical bond of CO_2 with the MOF components, has a higher activation energy and is more efficient for CO_2 kinetic capturing combined with pressure and temperature modulation. Thermally stable MOFs, such as the one simulated in this work, are promising for CO_2 chemisorption capturing and conversion through thermally driven reactions. In a recent publication,[8] the authors highlighted the importance of MOFs computational screening for discovering new promising materials for CO_2 capture but did neither include in their methods dynamics, reactivity, nor a fast identification of the crucial movements of the active components of the MOFs (the organic linkers) in supercell periodic models.

Therefore, descriptive/predictive computational methods capable of revealing atomic details and refined experimental characterization techniques play a crucial role in this context. From a computational point of view, most investigations were based on expensive quantum chemistry calculations at the density functional theory level.[9] Due to high computational costs, they were limited to simulating the material unit cells counting on periodic boundary conditions to mimic an infinite system. Considering the size of the crystallographic unit cells compared to the size and variability of the experimental material, this choice was restrictive, especially for evaluating the diffusion of guest molecules and linker movements, which were, thus, biased by the periodic images. The simulation

[a]CNR-ICCOM, Institute of Chemistry of Organometallic Compounds, Pisa 56124, Italy. E-mail: sapeptides@gmail.com
[b]CNR-IPCF, Institute of Chemical and Physical Processes, Pisa 56124, Italy
[c]Department of Pharmacy, University of Pisa, Pisa 56126, Italy

†Electronic supplementary information (ESI) available: Histogram of the orientations of CO_2 inside a MOF channel; a plot of the motion of CO_2 along the channel as a function of time, plot of the motion CO_2 along the channel as a function of time flanked with the torsional angle evolution plot of the linkers close by; QC calculations to estimate the energy barriers, details of the PCA analysis. Structures and data used in this work are available from the authors upon reasonable request. Video showing the CO_2 diffusion process in a MOF channel (CO2diffusion.mp4). See DOI: https://doi.org/10.1039/d3nr02760k

methods based on pre-parametrized force fields could be a more appropriate and successful solution.[10–14] Still, they could be challenged by the description of the combination of the inorganic and organic components and the necessity to simulate bond breaking and formation that is crucial for evaluating possible bonds of the guest to the frameworks and reactions involving the loaded species. The loading is usually carried out after desolvating the MOF that often accommodates water molecules (or other solvents) during the synthesis process because of its open-framework nature. Emptying the framework can favor the entrapment of other guest species in the core of the material and promote the catalytic conversion of the molecules, as in the case of CO_2. Developing performant materials for high CO_2 capture is a very active field, and some promising MOFs have already been identified.[15,16] These are those where the adsorption/desorption of guest molecules can be modulated by the gate-opening/closing phenomenon, namely evolution from a closed to an open penetrable phase, and breathing effects, namely structural transformation due to atomic reorganizations caused by the interactions with the guest species (efficient for CO_2 separation).[17,18]

In a recent review,[19] Singh *et al.* highlighted a disadvantage of the structure flexibility that causes a pore size reduction upon solvent removal, disfavoring CO_2 adsorption. This implies that in flexible systems, it is necessary to modulate both the pressure and temperature (or apply external stimuli such as high electric fields capable of inducing smoother transition between different structural states) to finely regulate the pore size and control the gas's selectivity, diffusion, and entrapment. On the other hand, it was also observed that in MOF with organic ligands, structural flexibility could have a highly favorable impact on selective CO_2 capture and separation, even though also these cases require an external biasing. To improve these characteristics, examining the adsorption isotherms can help reveal the gate-opening effects and disclose the material's behavior (breathing behavior) under various capture conditions. Combined with theoretical modeling (*i.e.* molecular dynamics, grand canonical Monte Carlo simulations), such detection could predict more effective solutions and drive the design/development of tuned gate-opening systems. These are, for example, those based on metal atoms coordinated to the carboxylic acid organic linkers with selected chains.[20] Another aspect examined in ref. 19 is the presence of non-uniform pores with different dimensions that could improve selectivity and adsorption capability and the role played by the computational techniques in all these studies.

For example, modeling could be beneficial in predicting the unexpected adsorption of large molecules, experimentally observed, and their high diffusion inside a framework. This implies that flexibility modifies the diffusivity of gases through the porous network. The characterization and prediction of these events are relevant for disclosing the effects of the linkers selection on the adsorption/conversion process and tailoring their structure to regulate channels/pores size and their movements relative to those of the loaded guests.

We have already demonstrated in an earlier work[21] that the dynamics of a loaded MOF can be realistically simulated by resorting to periodic supercells and a reactive molecular dynamics (RMD) approach with a dedicated force field (ReaxFF paradigm).[22–24] Here, we have improved the model further, focusing on the details of the framework motions by including the principal component analysis (PCA) of the sampled configurations to extract the main movements of the MOF linkers and their concertations during the diffusion of the guests. We found inspiration from earlier studies related to biosystems that demonstrated the effective use of PCA to extract concerted motions from the simulation trajectories.[25–27]

Indeed, PCA splits a configurational space into high-dimensional domains of high-frequency independent movements and low-dimensional subdomains of significant concerted motions. These are obtained by decomposing the atomic fluctuations (positional deviations from a reference structure) into a set of principal components (PC). The reference is usually an average geometry calculated after superimposing the trajectory on a reference system to remove unneeded translational and rotational motions through least squares fitting. In our case, given the nature of our target, the PCA procedure was used unconventionally. This is because it was not applied to a single molecule, such as a protein or a DNA/RNA chain,[26] but to a more complex supramolecular system as done in an earlier paper of ours.[28] We restricted the analysis by superimposing the trajectories on the IBUs atoms, which were less influenced by the statistical noise. Diagonalization of the Cartesian coordinates covariance matrix produces eigenvectors related to the motion direction relative to the average (correlated displacements of the atoms) and eigenvalues representing the mean-square fluctuations of the systems along the corresponding eigenvectors (amplitudes of the motion). The eigenvectors with the higher eigenvalues are the dominant movements. If only a few PC can be used to explain most of the total variance, the motions are highly correlated. On the contrary, in the case of many PC, the movements are random.

Visualization of the motions described by the eigenvectors by projecting each sampled configuration onto those eigenvectors gave us an estimate of the width of the essential space explored by the system as a function of time.

We selected the F4_MIL140A(Ce) system (Fig. 1)[29] motivated by recent studies on its possible use in photocatalytic applications, built a model from the experimental data,[29] loaded it with CO_2 molecules, carried out RMD simulations, and the related analysis of the trajectories. We could identify possible CO_2 connections to the IBUs, characterize the channels, and disclose the details of the CO_2 diffusion pathways by mapping the CO_2 orientations, stationary stages, and the related movements of the linkers.

2 Methods

Before describing the computational methods, a brief introduction explaining the MOF structure is mandatory to connect

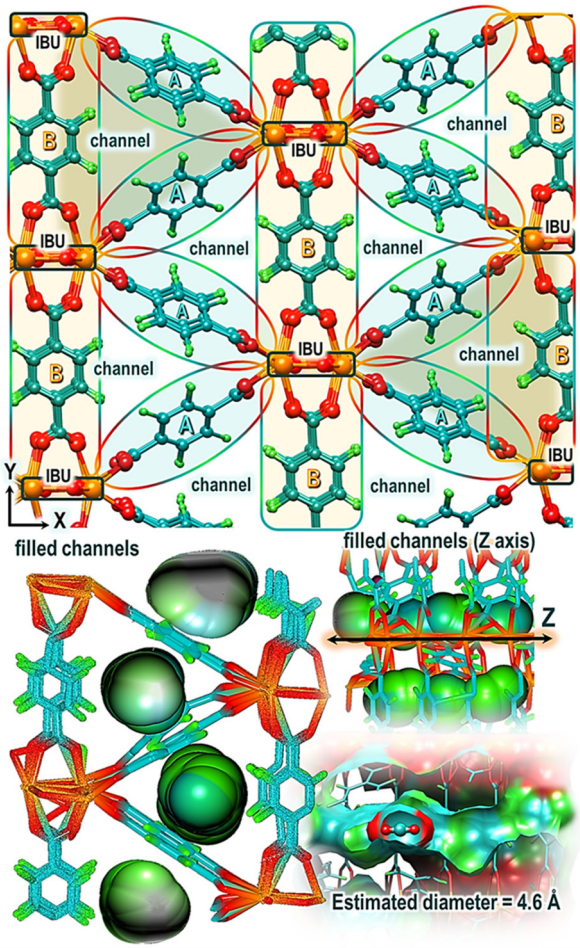

Fig. 1 Top: F4_MIL140A(Ce) structure. Color code: Ce – orange, O – red, C – dark cyan, F – green. Bottom: Shapes of the MOF channels (pipelines with varying widths of the cross sections) mapped through superimposed spheres (CAVER Analyst). On the right, a section of a channel containing a CO_2 molecule is visible.

the reported descriptions straightaway. The F4_MIL140A(Ce) structure contains one-dimensional ceria inorganic building units (IBU) aligned along the *Z* direction that are inter-connected through 2,3,5,6-tetrafluoro-1,4-benzene dicarboxylic acid molecules (Fig. 1). The carboxyl groups are coordinated to the metal centers (cerium atoms). The orientations of these linkers are of two different types, almost perpendicular to the plane containing the IBUs (B linkers) and inclined to it by about 30 degrees (A linkers). In the A arrangement, the linkers are located side by side but rarely coplanar (temporary high-energy structures). In contrast, they form a line of almost stacked arrangements in the B orientation. This triangle-like distribution generates long cylindric-like channels (with an average diameter of approximately 4.6 Å) running along the *Z* direction. In the optimized configurations, the perfluorinated phenyl rings are rotated relative to the carboxyl groups by about 46 degrees (Fig. 1). D'Amato and co-workers have described this MOF's experimental structure and properties in ref. 29. We used the crystallographic structure deposited in the Cambridge Crystallographic Data Centre (entry CCDC-1855704) as starting geometry for building our models.

2.1 Model building

First, we optimized the downloaded data with the Quantum Espresso (QE) code,[30] considering a cell size of 25.8 × 11.6 × 8.1 $Å^3$ and angles of 90°, 96°, and 90° at the density functional theory level (DFT) using ultrasoft pseudopotentials and the generalized gradient approximation (GGA) with the Perdew–Burke–Ernzerhof (PBE) functional,[31] and cutoff energy of 600 eV. We applied periodic boundary conditions in all directions. We created a supramolecular MOF model by replicating the QE-optimized geometry three times in *x*, *y*, and *z* directions (3 × 3 × 3 supercell = 77.5 × 34.8 × 24.2 $Å^3$) after removing the water molecules present in the original data.

Then, we built a configuration filled with CO_2 molecules. To insert CO_2, we prepared an equilibrated CO_2 "solvation" box at a 98 kg m^{-3} density through repeated *NVT*, *NPT*, and *NVE* simulations using the Amber16 MD package.[32] The final model was energy minimized with the ReaxFF program in the ADF package[33] based on the specialized force fields developed in earlier works.[34–36] A few details of the force field refinement and validation are reported at the end of the ESI.†

The model contains 7–8 CO_2 per unit cell (QE geometry). This configuration was employed to simulate guest and linker dynamics at ambient temperature and pressure through ReaxFF molecular dynamics.

2.2 Reactive molecular dynamics simulations (RMD)

After energy minimization, the model was equilibrated at T = 298 K and then sampled in the *NVT* ensemble for about 600 ps. The time step was set to 0.20 fs. The temperature was controlled through the Anderson thermostat with a relaxation constant of 0.1 ps, and system structures were saved every 0.02 ps. The collected data were analyzed considering distance and angle distributions and their evolution during the dynamics.

We used the principal component analysis (PCA)[37,38] unconventionally to disclose the main motions of the linkers and the type of concertations responsible for the diffusive behavior of the CO_2 molecules in the MOF channels. The coordinated movements of the A and B linkers were transformed into a set of orthogonal vectors to identify the dominant reorientations by eliminating the rotational/translational motions (translation of all the sampled snapshots to the average geometrical center of the selected portion of the system and performing the least squares fit superimposition onto the average configuration). In the case of ring rotations, we chose the carboxyl oxygens and the coordinated cerium atoms as the fitting atoms. The eigenvectors of the covariance matrix gave a vectorial description of each motion component and its directions. The corresponding eigenvalues were the weights of each movement. The trajectory projection on a particular eigenvector highlighted the time-dependent moves of the rotational/vibrational mode and was used for animations. We rendered the movement directions through porcupine plots highlighting

the projections on the main principal components (first three modes). The tips of the arrows on each atom indicate the motion direction, while the spikes' lengths represent the motion amplitude.

2.3 Quantum chemistry calculations (QC)

QC calculations on cluster models were used to estimate the energy barriers of the ring rotations. Constrained optimizations were performed at the DFT level using the M062X functional and the 6-31G(d,p) basis set with the Gaussian16 code.[39]

3 Results and discussion

A representative snapshot of the loaded MOF extracted from the simulations at T = 298 K is shown in Fig. 2. Examination of the picture and the distribution of the CO_2 oxygen distances from the metal centers indicates strongly orientational effects of CO_2 molecules around the Ce atoms within the first coordination shell of Ce. The peak at about 2.2 Å corresponds to bonded CO_2 with an orientation of about 50 degrees relative to the axis of the channel (Z direction – Fig. 1 and S1†), located in the region between the lines of A and B linkers. The peak at 2.37 Å can be assigned to those connections where the molecule has an inclination of about 80 degrees and is hindered by the linkers to get closer to Ce atoms. From these positions, the molecule can move quickly into the channel (in the middle of the triangular regions – Fig. 2 and ESI Video†). These results agree with the general picture of the diffusion process reported in the literature for MOF systems.[40] We estimated the shapes of the channels through the CAVER analysis[41] that identified pockets, cavities, and tunnels by filling them with superimposed spheres of variable radius (Fig. S1†). The characteristics of these channels are a low curvature and an alignment almost parallel to the IBU units (Z direction).

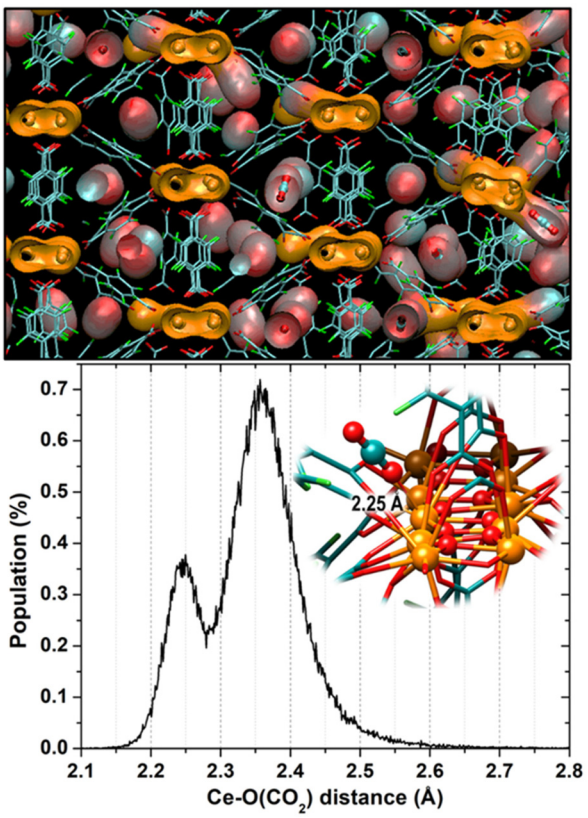

Fig. 2 The top image is a representative snapshot extracted from the simulations at T = 298 K. IBUs (orange), and CO_2 (light red) are rendered by solvent-accessible surfaces (SAS), whereas sticks depict the linkers. Color code: Ce – orange, O – red, C – dark cyan, F – green. The plot shows the distribution of the CO_2 oxygen distances from the Ce atoms sampled during the simulations.

A section of a typical channel containing a CO_2 molecule is displayed in Fig. 1. The diameter of the various portions varied during the simulations in line with the orientations of the linkers' rings (mainly of A-type) because they formed two sides of the triangle and were more mobile. Instead, the B linkers were practically aligned on the shorter side. Checking the different contributions (cumulative contributions of the filling spheres) obtained with CAVER,[41] we estimated an average diameter of approximately 4.6 Å, which reasonably agrees with the data of the static experimental characterization.[29]

A typical diffusion pathway of a few CO_2 molecules inside a channel and the related activity of the MOF linkers can be visualized in the ESI Video.† The collected snapshots span about 250 ps (final portion of the equilibrated trajectory), sufficient to recognize all the process stages and give a stable and statistically reliable picture of the essential subspace on the total timescale of the simulations. Then, we focused on one of these molecules only for a finer characterization. Inspection of the sequence suggests that CO_2 spent quite a long time on the flat rings, lulled by their librations, and could go back and forth in the channel, frequently changing its orientation, which was preferentially at 20 degrees to the Z axis (Fig. S1†).

As confirmed by the position occupation density shown in Fig. 3, it is clear that the most convenient location was close to the tunnel's center (between two A linker pairs), where the unfavorable interactions with the perfluorinated rings are minimal. However, after a while (variable time intervals in the range of 25–120 ps), specific combinations of the ring librations pushed the molecules to other channel regions, and the process was repeated (step-by-step diffusion along Z). A pictorial representation of the entire journey of the selected CO_2 is visible in Fig. 4. There, all the collected CO_2 positions are displayed (ball and sticks), and the flat A linkers pairs are identified by the average planes (green disks) containing both rings.

The journey's starting point is from the third Ce on the right, where the CO_2 was coordinated, and the ending location is on the opposite side, close to the slightly rotated A linker (magenta plane) that probably caused a deviation of the molecule.

Fig. S2† shows the path traveled along Z by four different CO_2 molecules. The longest distance traveled without interruptions was approximately 1 nm. The plots have been smoothed

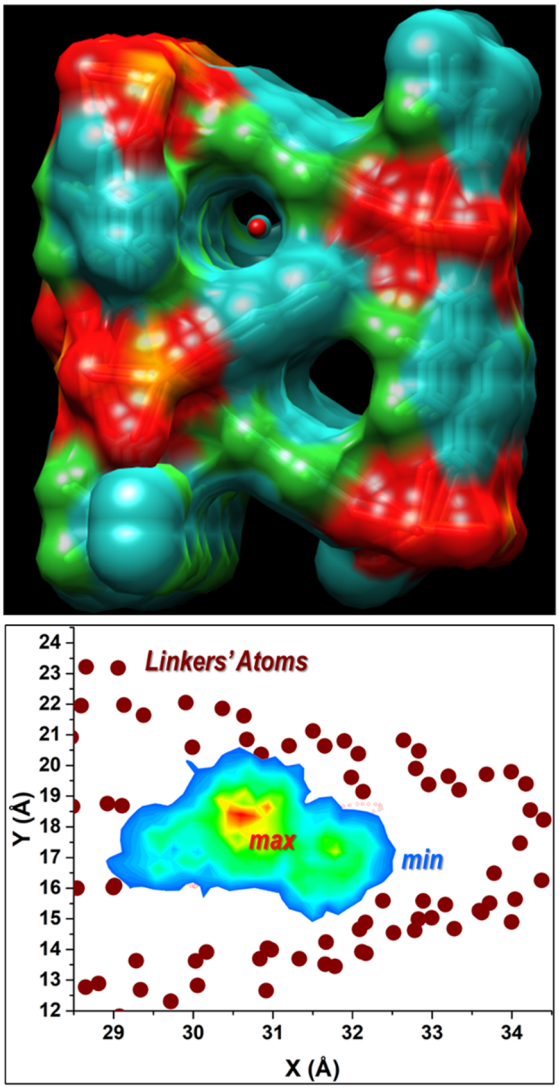

Fig. 3 The top image shows a CO_2 molecule at the center of a channel (SAS). The framework structure is rendered by SAS colored according to the atom type. Color code: Ce – orange, O – red, C – dark cyan, F – green. The plot shows the distribution density (colored contours) of CO_2 positions in the plane perpendicular to the channel axis (center of mass *x*, *y* coordinates) explored during the simulation. Maximum and minimum densities are red and blue contours, respectively. The brown circles are the atoms of the linkers.

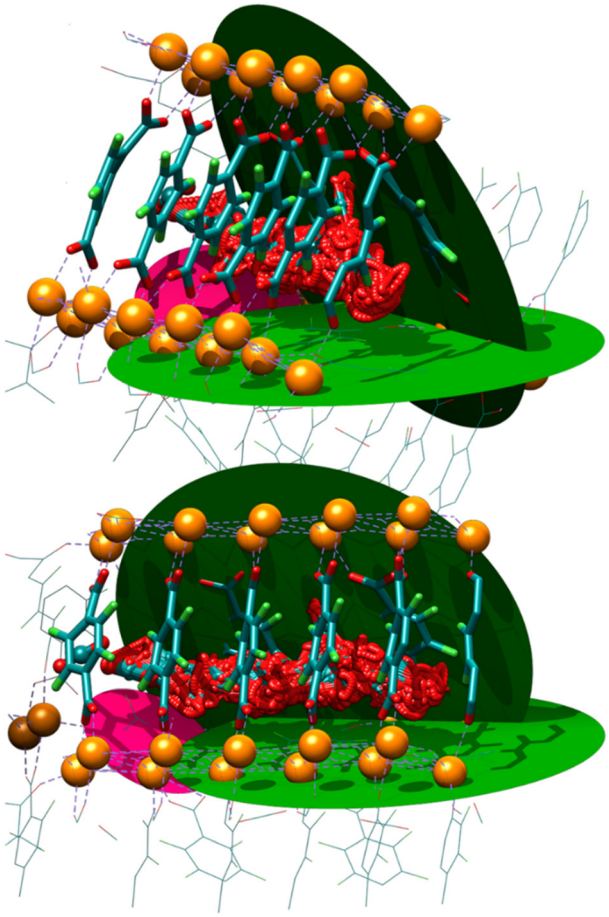

Fig. 4 Two views of the channel containing all the diffusing CO_2 coordinates superimposed (oxygen balls) to highlight the 3D path. The channel is defined by the two green disks containing the A linker rings and by the lined stacked B linkers (sticks). Color code: Ce – orange, O – red, C – dark cyan, F – green. The magenta disk identifies a slightly rotated ring (A linker) that could induce a deviation of the molecule. The final position of CO_2 is on the left, above the magenta disk.

to disclose relatively *Z*-stationary periods. The oscillations were quite pronounced, and their trend was probably connected to the amplitude of the librations of the closer phenyl rings. The arrows indicate longer routes, and their orientation, the tendency to retrace parts of the channel. The motion was very complex and hardly connected to evident librations. Thus, we checked possible connections by analyzing the evolution of the torsional angles of the A linkers, which had more marked librations than the B ones (Fig. S3†). Comparison of the various trends suggests no apparent correlation with the *Z*-path of CO_2, even though the stationary regions seem connected with the reduction of the oscillations of the torsional of one of the A linkers.

The angle variations were consistently lower than 90 degrees (confirming librations), and we could not observe a flip tendency even though, from a rough estimate, the rotational barriers were probably lower than 10 kcal mol^{-1} (Fig. S4†), which was comparable with local maximum energy fluctuations observed during the dynamics.

As the final analysis, we resorted to essential dynamics to unravel the detailed movements of phenyl rings and identify the main concerted motions of the A and B pairs during the simulations.

First, we removed the rotational/translational movements we were not interested in by superimposing all the snapshots of the extracted channel portion on the cerium and carboxyl oxygens and then performed an RMS best fit to the reference structure (averaged coordinates). The results of the RMS fit and the eigenvalues of the modes are reported in Fig. 5 and Table S1 of the ESI.†

In Fig. 5 and S5,† the motion along the first two principal components is displayed through superimposed structures

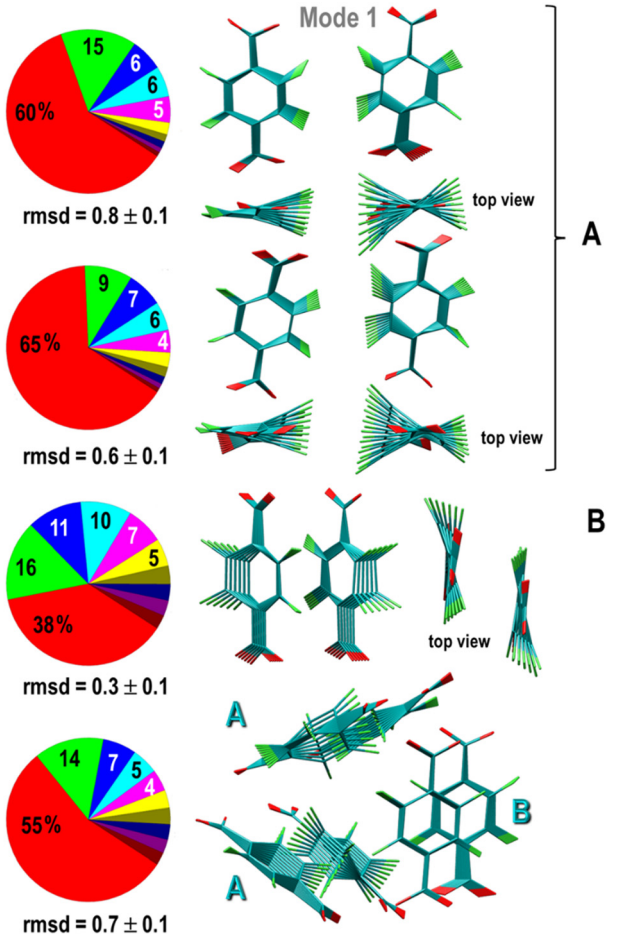

Fig. 5 Linkers pairs forming a section of the channel. From top to bottom: type A, type A, type B. Dominant mode (mode 1 – red, mode 2 – green, mode 3 – blue, *etc.*) identified by PCA (superimposing all the snapshots on the coordinated Ce atoms and carboxyl oxygens – rmsd values are reported). Structure color code: O – red, C – dark cyan, F – green.

defining the animation (the minimum and maximum values were selected considering the distributions of the principal component projections shown in Fig. S6†). As can be noticed, the values reflect the stacked B linkers' restricted dynamic tendency and the A linkers' ample libration at their interface.

The first ten eigenvalues correspond to concerted motions quickly decreasing in amplitude toward more localized fluctuations. The first two components account for more than 54% of the observed movement (Table S1†). The motions along the first three eigenvectors were obtained by projecting all the collected structures on each eigenvector, and the histograms of the fluctuations are shown in Fig. S6.†

These plots can give an idea of the degree of anharmonicity of the motions considering that Gaussian distributions identify harmonic movements. As we can see, almost all the modes are essentially anharmonic, and the presence of various peaks suggests multiple arrangements of the structures. Examination of the isolated A pairs reveals slightly different reorganizations of the systems due to the dissimilar surroundings and perturbations but similar types of motions (visualized as superimposed structures spanning the whole libration). Instead, a sort of harmonicity and concertation is apparent in the case of B linkers (mainly mode 2 and mode 3) that exhibit a monomodal fluctuation profile with smaller amplitudes. These data suggest the independence of the three sides of the channel (referring to the triangular organization scenario described in ref. 29).

By inspecting mode 1 in the six-linker complex (Fig. S6†) and separate A linkers (Fig. S6b and c†), it can be seen that the A linkers can adopt two somewhat diverse configurations (dominant peaks). The shoulder could be due to the added local librations of the carboxyl groups, and it is more evident in one of the pairs (Fig. S6b†). As expected, the movements of the A linkers dominate the motion of the whole complex, and the asymmetric librations of the perfluorinated phenyl rings (more evident at their interface where the fluorine atoms interact) are probably responsible for the kicks pushing CO_2 along the MOF channels. However, all the motions seem concerted. This was confirmed by analyzing the other components (modes two and three), where we found part of the motion described in mode one.

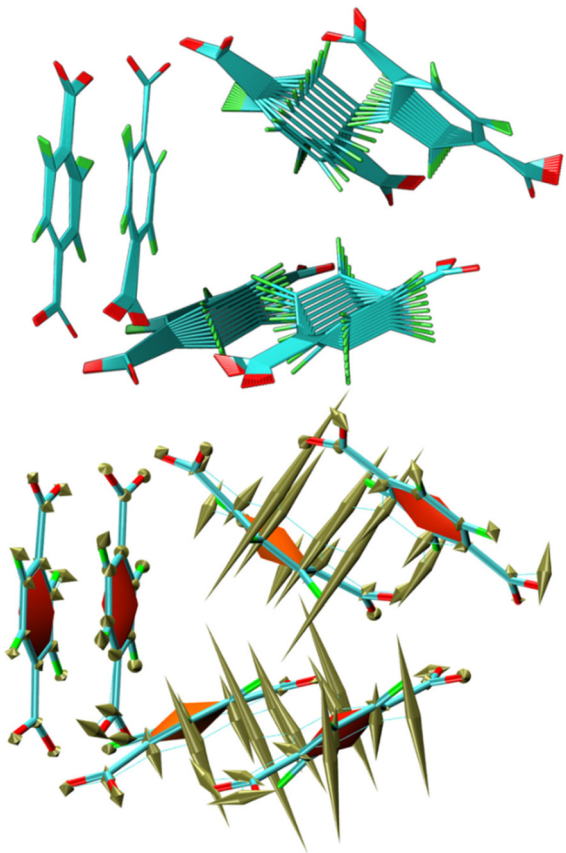

Fig. 6 Linkers pairs forming a section of the channel. Mode 1 identified by PCA (superimposing all the snapshots on the coordinated Ce atoms and carboxyl oxygens – rmsd values are reported in Fig. S5†). Porcupine rendering of the main linker movements. The superimposed structures depict the total libration of the linkers. Color code: C = dark cyan, O = red, F = green.

The motion of the linkers was visualized through structure superimpositions, and porcupine plots[42] that show the direction and magnitude of the selected eigenvectors for each linker atom. The first and second modes of the six-ring complex are shown in Fig. 6 and 7, respectively, whereas the third mode is displayed in Fig. S7 of the ESI.†

Again, the partial rotation of the A linker rings is the dominant motion, and the carboxyl group librations are readjustment toward the Ce atoms. The range of the ring rotations is more extended in the inter-linker region of the nearest linkers because they tend to avoid the unfavorable coplanar arrangement, and thus, their reorientations are correlated. The correlation of the B linkers' motion instead is due to their stacked arrangements that partially hinder their librations.

This analysis shed light on the correlation and concertation of the linker movements and could be effectively used for local predictions on the dynamics of the gate-opening/closing phenomenon. Indeed, we could use the pseudo-trajectory of motion along the first PC (mode 1) to predict the librations' effect on the channel's variability by visualizing the geometries corresponding to average configuration and maximum librations. These are shown in Fig. S8 of the ESI.† It is clear that only when the phenyl rings of the adjacent linkers (A-type) are practically coplanar, the channel is almost straight with a uniform section (maximum opening). Instead, the partial rotations of the phenyl rings are responsible for the formation of bottlenecks, which render the channel more tortuous and narrow (Fig. S8a–c†) and thus less accessible for a fast CO_2 diffusion along the z direction.

A rough estimate of the diffusion coefficient of a few CO_2 molecules was obtained from the trajectory calculating the mean square displacements (MSD) of their coordinates, from the initial positions, along the z direction according to ref. 43–45. Even though it was not accurately determined, it could provide an order of magnitude (about 3×10^{-9} m^2 s^{-1}) comparable to that of liquid water (2.3×10^{-9} m^2 s^{-1}),[43] and in line with the values found for other MOFs.[46]

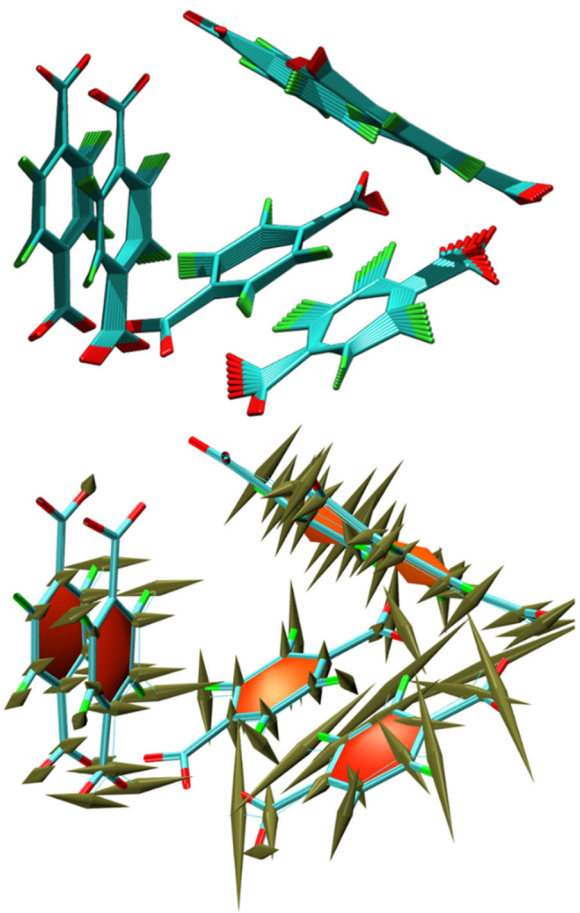

Fig. 7 Linkers pairs forming a section of the channel. Mode 2 identified by PCA (superimposing all the snapshots on the coordinated Ce atoms and carboxyl oxygens – rmsd values are reported in Fig. S5†). Porcupine rendering of the main linker movements. Structure color code: O – red, C – dark cyan, F – green.

4 Conclusions

In sum, the computational strategy we have defined and all the analysis tools we have employed could provide a detailed realistic scenario of the flexibility of the structure in terms of principal librations of the F4_MIL140A(Ce) MOF ligands, which determined the fluctuation of the channels and pores, in connections with the dynamics of the loaded guest species (CO_2 molecules) in terms of diffusivity inside the channels and adsorption onto the metal sites. We could observe modest breathing of the framework (Fig. S9†) in line with the chosen simulation conditions (*NVT* instead of *NPT* ensemble). The carboxyl oxygens of the ligands remained essentially coordinated to the metal centers. Still, as evidenced by the principal component analysis, they could librate about the C–C axes, frequently changing their distance from the Ce atoms. Given the ligands' relative positions, concerted movements acted on the dynamics of the CO_2 molecules. The diffusion of CO_2 occurred mainly in the center of the long channel extending along the whole z direction but was perturbed by the ring librations, which were also perturbed by the interactions with the loaded species. Thus, the CO_2 molecules often changed the direction of their motion going back and forth in the canals. The whole effect was a sort of unbiased entrapment (having not applied specific temperatures and pressures) at the simulated ambient pressure and temperature. We could disclose, characterize and predict the gate-opening and closing phenomenon through the principal component analysis on a main channel section and show it in a short movie. The variability of the channel sections, which was regulated by the concerted librations of the ligand rings, determined the inversion of the directions of the motion (retroactive deviation from the central axis of the channel) and a consequential slowdown of the CO_2 velocity. Due to specific concerted reorientations of the ligand, we observed that some CO_2 molecules could migrate into adjacent tunnels and diffuse there. Instead, the libration of the carboxyls coordinated to the metal center could leave space for the

coordination of one of the CO_2 oxygens to the Ce atoms determining temporary adsorption. The short lifetime of these positions depended on the CO_2 self-interactions. A-type linkers were responsible for the dominant movements in the MOF and determined the variation of the tunnels, whereas B-type linkers remained more aligned and compact.

CO_2 was only weakly adsorbed on the metal centers and had the tendency to slowly diffuse, after a few picoseconds, due to collisions with other molecules, in the MOF channels for a period depending on the local perturbations.

Our results agree satisfactorily with experimental and theoretical studies, and they are very promising for extending the simulations/analysis procedure to other systems. This methodology can be beneficial for interpreting the experimental results and predicting appropriate substitution to improve the materials' performance.

Conflicts of interest

There are no conflicts to declare.

Notes and references

1 Q. Wang and D. Astruc, State of the Art and Prospects in Metal-Organic Framework (MOF)-Based and MOF-Derived Nanocatalysis, *Chem. Rev.*, 2020, **120**(2), 1438–1511.
2 E. Martínez-Ahumada, A. López-Olvera, V. Jancik, J. E. Sánchez-Bautista, E. González-Zamora, V. Martis, D. R. Williams and I. A. Ibarra, MOF Materials for the Capture of Highly Toxic H_2S and SO_2, *Organometallics*, 2020, **39**, 883–915.
3 J. Hwang, A. Ejsmont, R. Freund, J. Goscianska, B. V. K. J. Schmidt and S. Wuttke, Controlling the morphology of metal-organic frameworks and porous carbon materials: metal oxides as primary architecture-directing agents, *Chem. Soc. Rev.*, 2020, **49**, 3348–3422.
4 S. Dutta and S. Lee, Metal-organic framework based catalytic nanoreactors: synthetic challenges and applications, *Mater. Chem. Front.*, 2021, **5**, 3986–4021.
5 Z. Yu, D. M. Anstine, S. E. Boulfelfel, C. Gu, C. M. Colina and D. S. Sholl, Incorporating Flexibility Effects into Metal-Organic Framework Adsorption Simulations Using Different Models, *ACS Appl. Mater. Interfaces*, 2021, **13**(51), 61305–61315.
6 X. Gao, F. Ge and H. Zheng, Improving the Stability and Visualizing the Structural Transformation of the Stimuli-Responsive Metal-Organic Frameworks (MOFs), *Inorg. Chem.*, 2020, **59**(7), 5093–5098.
7 J. Buckingham, T. R. Reina and M. S. Duyar, Recent advances in carbon dioxide capture for process intensification, *Carbon Capture Sci. Technol.*, 2022, **2**, 100031.
8 G. Avci, I. Erucar and S. Keskin, Do New MOFs Perform Better for CO_2 Capture and H_2 Purification? Computational Screening of the Updated MOF Database, *ACS Appl. Mater. Interfaces*, 2020, **12**, 41567–41579.
9 A. Gonzalez-Nelson, F.-X. Coudert and M. A. van der Veen, Rotational Dynamics of Linkers in Metal-Organic Frameworks, *Nanomaterials*, 2019, **9**, 330.
10 V. J. Witherspoon, L. M. Yu, S. Jawahery, E. Braun, S. M. Moosavi, S. K. Schnell, B. Smit and J. A. Reimer, Translational and Rotational Motion of C8 Aromatics Adsorbed in Isotropic Porous Media (MOF-5): NMR Studies and MD Simulations, *J. Phys. Chem. C*, 2017, **121**, 15456–15462.
11 M. Heshmat, Alternative Pathway of CO_2 Hydrogenation by Lewis-Pair-Functionalized UiO-66 MOF Revealed by Metadynamics Simulations, *J. Phys. Chem. C*, 2020, **124**, 10951–10960.
12 G. Avci, S. Velioglu and S. Keskin, High-Throughput Screening of MOF Adsorbents and Membranes for H_2 Purification and CO_2 Capture, *ACS Appl. Mater. Interfaces*, 2018, **10**, 33693–33706.
13 Y. Magnin, E. Dirand, A. Orsikowsky, M. Plainchault, V. Pugnet, P. Cordier and P. L. Llewellyn, A Step in Carbon Capture from Wet Gases: Understanding the Effect of Water on CO_2 Adsorption and Diffusion in UiO-66, *J. Phys. Chem. C*, 2022, **126**, 3211–3220.
14 P. B. Shukla and J. K. Johnson, Impact of Loading-Dependent Intrinsic Framework Flexibility on Adsorption in UiO-66, *J. Phys. Chem. C*, 2022, **126**(41), 17699–17711.
15 T. M. McDonald, W. R. Lee, J. A. Mason, B. M. Wiers, C. S. Hong and J. R. Long, Capture of carbon dioxide from air and flue gas in the alkylamine-appended metal-organic framework mmen-Mg_2(dobpdc), *J. Am. Chem. Soc.*, 2012, **134**, 7056–7065.
16 T. M. McDonald, J. A. Mason, X. Kong, E. D. Bloch, D. Gygi, A. Dani, V. Crocella, F. Giordanino, S. O. Odoh, W. S. Drisdell, B. Vlaisavljevich, A. L. Dzubak, R. Poloni, S. K. Schnell, N. Planas, K. Lee, T. Pascal, L. F. Wan, D. Prendergast, J. B. Neaton, B. Smit, J. B. Kortright, L. Gagliardi, S. Bordiga, J. A. Reimer and J. R. Long, Cooperative insertion of CO_2 in diamine-appended metal-organic frameworks, *Nature*, 2015, **519**, 303–308.
17 D. Fairen-Jimenez, S. A. Moggach, M. T. Wharmby, P. A. Wright, S. Parsons and T. J. Düren, Opening the gate: framework flexibility in ZIF-8 explored by experiments and simulations, *J. Am. Chem. Soc.*, 2011, **133**, 8900–8902.
18 G. Férey and C. Serre, Large breathing effects in three-dimensional porous hybrid matter: facts, analyses, rules and consequences, *Chem. Soc. Rev.*, 2009, **38**, 1380–1399.
19 G. Singh, J. Lee, A. Karakoti, R. Bahadur, J. Yi, D. Zhao, K. AlBahily and A. Vinu, Emerging trends in porous materials for CO_2 capture and conversion, *Chem. Soc. Rev.*, 2020, **49**, 4360–4404.
20 S.-M. Hyun, J. H. Lee, G. Y. Jung, Y. K. Kim, T. K. Kim, S. Jeoung, S. K. Kwak, H. R. Moon and D. Moon, *Inorg. Chem.*, 2016, **55**, 1920–1925.
21 J. Piatek, T. M. Budnyak, S. Monti, G. Barcaro, R. Gueret, E. S. Grape, A. Jaworski, A. K. Inge, B. V. M. Rodrigues and

A. Slabon, Toward Sustainable Li-Ion Battery Recycling: Green Metal-Organic Framework as a Molecular Sieve for the Selective Separation of Cobalt and Nickel, *ACS Sustainable Chem. Eng.*, 2021, **9**, 9770–9778.

22 A. C. T. van Duin, S. Dasgupta, F. Lorant and W. A. Goddard, ReaxFF: A reactive force field for hydrocarbons, *J. Phys. Chem. A*, 2001, **105**, 9396–9409.

23 K. Chenoweth, A. C. T. van Duin and W. A. Goddard, ReaxFF reactive force field for molecular dynamics simulations of hydrocarbon oxidation, *J. Phys. Chem. A*, 2008, **112**, 1040–1053.

24 T. Senftle, S. Hong, M. Islam, *et al.*, The ReaxFF reactive force-field: development, applications and future directions, *npj Comput. Mater.*, 2016, **2**, 15011.

25 A. Amadei, A. B. Linssen and H. J. Berendsen, Essential dynamics of proteins, *Proteins*, 1993, **17**, 412–425.

26 T. Meyer, C. Ferrer-Costa, A. Perez, M. Rueda, A. Bidon-Chanal, F. J. Luque, C. A. Laughton and M. Orozco, Essential dynamics: a tool for efficient trajectory compression and management, *J. Chem. Theory Comput.*, 2006, **2**, 251–258.

27 D. K. Chakravorty, B. Wang, C. W. Lee, D. P. Giedroc and K. M. Merz, Simulations of Allosteric Motions in the Zinc Sensor CzrA, *J. Am. Chem. Soc.*, 2012, **134**, 3367–3376.

28 S. Monti, I. Cacelli, A. Ferretti, G. Prampolini and V. Barone, DNA hybridization mechanism on silicon nanowires: a molecular dynamics approach, *Mol. BioSyst.*, 2010, **6**, 2230–2240.

29 R. D'Amato, A. Donnadio, M. Carta, C. Sangregorio, D. Tiana, R. Vivani, M. Taddei and F. Costantino, Water-Based Synthesis and Enhanced CO_2 Capture Performance of Perfluorinated Cerium-Based Metal-Organic Frameworks with UiO-66 and MIL-140 Topology, *ACS Sustainable Chem. Eng.*, 2019, **7**, 394–402.

30 P. Giannozzi, S. Baroni, N. Bonini, *et al.*, QUANTUM ESPRESSO: A modular and open-source software project for quantum simulations of materials, *J. Phys.: Condens. Matter*, 2009, **21**, 395502.

31 J. P. Perdew, K. Burke and M. Ernzerhof, Generalized Gradient Approximation Made Simple, *Phys. Rev. Lett.*, 1996, **77**, 3865–3868.

32 D. A. Case, R. M. Betz, D. S. Cerutti, T. E. Cheatham, III, T. A. Darden, R. E. Duke, T. J. Giese, H. Gohlke, A. W. Goetz, N. Homeyer and S. Izadi, *et al.*, *AMBER 2016*, University of California, San Francisco, 2016.

33 E. J. Baerends, *et al.*, *ADF, adf2019.102 SCM*, Theoretical Chemistry, Vrije Universiteit, Amsterdam, The Netherlands, **https://www.scm.com**.

34 P. Broqvist, J. Kullgren, M. J. Wolf, A. C. T. van Duin and K. Hermansson, ReaxFF Force-Field for Ceria Bulk, Surfaces, and Nanoparticles, *J. Phys. Chem. C*, 2015, **119**, 13598–13609.

35 G. Barcaro, L. Sementa, S. Monti, V. Carravetta, P. Broqvist, J. Kullgren and K. Hermansson, Dynamical and Structural Characterization of the Adsorption of Fluorinated Alkane Chains onto CeO_2, *J. Phys. Chem. C*, 2018, **122**, 23405–23413.

36 L. Brugnoli, M. C. Menziani, S. Urata and A. Pedone, Development and Application of a ReaxFF Reactive Force Field for Cerium Oxide/Water Interfaces, *J. Phys. Chem. A*, 2021, **125**, 5693–5708.

37 A. Amadei, A. B. Linssen and H. J. Berendsen, Essential dynamics of proteins, *Proteins*, 1993, **17**, 412–425.

38 T. Meyer, C. Ferrer-Costa, A. Perez, M. Rueda, A. Bidon-Chanal, F. J. Luque, C. A. Laughton and M. Orozco, Essential dynamics: a tool for efficient trajectory compression and management, *J. Chem. Theory Comput.*, 2006, **2**, 251–258.

39 M. J. Frisch, G. W. Trucks, H. B. Schlegel, G. E. Scuseria, M. A. Robb, J. R. Cheeseman, G. Scalmani, V. Barone, G. A. Petersson, H. Nakatsuji, X. Li, M. Caricato and A. V. Marenich, *et al.*, *Gaussian 16, Revision C.01*, Gaussian, Inc., Wallingford, CT, 2016.

40 M. Ding, R. W. Flaig, H.-L. Jiang and O. M. Yaghi, Carbon capture and conversion using metal-organic frameworks and MOF-based materials, *Chem. Soc. Rev.*, 2019, **48**, 2783–2828.

41 A. Jurcik, D. Bednar, J. Byska, S. M. Marques, K. Furmanova, L. Daniel, P. Kokkonen, J. Brezovsky, O. Strnad, J. Stourac, A. Pavelka, M. Manak, J. Damborsky and B. Kozlikova, CAVER Analyst 2.0: Analysis and Visualization of Channels and Tunnels in Protein Structures and Molecular Dynamics Trajectories, *Bioinformatics*, 2018, **34**, 3586–3588.

42 K. Tai, T. Shen, R. H. Henchman, Y. Bourne, P. Marchot and J. A. McCammon, Mechanism of acetylcholinesterase inhibition by fasciculin: a 5-ns molecular dynamics simulation, *J. Am. Chem. Soc.*, 2002, **124**, 6153–6161.

43 M. Holz, S. R. Heil and A. Sacco, Temperature-Dependent Self-Diffusion Coefficients of Water and Six Selected Molecular Liquids for Calibration in Accurate ^{1}H NMR PFG Measurements, *Phys. Chem. Chem. Phys.*, 2000, **2**, 4740–4742.

44 W. Humphrey, A. Dalke and K. Schulten, VMD – Visual Molecular Dynamics, *J. Mol. Graphics*, 1996, **14**, 33–38.

45 T. Giorgino, Computing diffusion coefficients in macromolecular simulations: the Diffusion Coefficient Tool for VMD, *J. Open Source Softw.*, 2019, **4**, 1698.

46 T. M. Tovar, J. Zhao, W. T. Nunn, H. F. Barton, G. W. Peterson, G. N. Parsons and M. D. LeVan, Diffusion of CO_2 in Large Crystals of Cu-BTC MOF, *J. Am. Chem. Soc.*, 2016, **138**(36), 11449–11452.